Characterization of residual stresses generated during inhomogeneous plastic deformation

T Lorentzen[1], **T Faurholdt**[2], **B Clausen**[1] and **J Danckert**[2]
[1]Materials Research Department, Risø National Laboratory, Roskilde, Denmark
[2]Department of Production, Aalborg University, Denmark

Abstract: Residual stresses generated by macroscopic inhomogeneous plastic deformation are predicted by an explicit finite element (FE) technique. The numerical predictions are evaluated by characterizing the residual elastic strains by neutron diffraction using two different (*hkl*) reflections. Intergranular residual elastic strains between subsets of grains are predicted numerically and verified by neutron diffraction. Subsequently, the measured residual strain profiles in the test samples are modified by the intergranular strains and compared to the engineering predictions of the FE technique. Results compare well and verify the capability of the numerical technique as well as the possibilities of experimental validation using neutron diffraction. The presented experimental and numerical approach will subsequently be utilized for the evaluation of more complicated plastic deformation processes resembling forming operations.

Keywords: residual stresses, plastic deformation, FE technique, neutron diffraction

NOTATION

c_i	acoustic wave speed
$\mathbf{C}$	damping matrix
$\boldsymbol{d}$	displacement vector
$\dot{\boldsymbol{d}}_n$	velocity vector
$\ddot{\boldsymbol{d}}_n$	acceleration vector
$\dddot{\boldsymbol{d}}_n$	time derivative of the acceleration vector
d^{hkl}	lattice spacing
d_0^{hkl}	lattice spacing in virgin material
E	Young's modulus
$\boldsymbol{F}^{\text{ext}_n}$	external force vector
$\boldsymbol{F}_n^{\text{int}}$	internal force vector
$\mathbf{K}$	stiffness matrix
L_i	characteristic element length
$\mathbf{M}$	mass matrix
n_{nodes}	number of nodes in an element
Δt	time step
$\Delta t_{\text{Courant}}$	critical time step
Γ	anisotropy factor
$\delta_{\alpha\beta}$	Kronecker delta
ε	residual elastic strain
λ	eigenvalue
ρ_i	mass density
ω_{max}	highest frequency of FE mesh

Subscript *n* denotes the *n*th time step and subscript *i* denotes the *i*th element. Superscript *hkl* refers to the *hkl* Bragg reflection given by Miller's indices.

1 INTRODUCTION

Most forming operations used in industry involve some degree of inhomogeneous plastic deformation, leading to the generation of residual stresses which may be detrimental to the structural integrity of the part. Residual stresses may be predicted using numerical techniques like the finite element (FE) technique; especially for forming operations involving very large deformations explicit FE codes have grown popular. The simulation of forming operations involves some parameters that are non-trivial to quantify; i.e. a process parameter like friction behaviour may need to be estimated and the constitutive behaviour of the material at processing temperatures and degrees of deformation may need to be extrapolated from uniaxial materials data. Hence, the numerical results are prone to be uncertain and an experimental evaluation of such predictions is called for. The residual strains lend themselves to experimental evaluation by the novel technique of neutron diffraction, which can be used in a non-destructive manner to quantify the bulk distribution of elastic lattice strains (see reference [1]). The aim of this work is to study the evolution of residual stresses during a complex sheet metal-forming operation like deep drawing. However, this is approached through a three-step process with increasing complexity
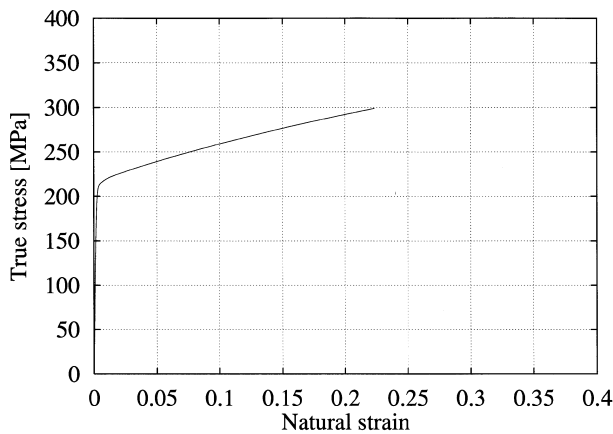
Fig. 1 True stress–strain curve for pure copper

both in the forming process and in the experimental evaluation of the stress distributions. The present work constitutes the first part of the study and focuses on a very simple geometry and deformation process, namely a tensile testing specimen with an inhomogeneous plastic deformation introduced by the design of the specimen waist section.

2 THE SPECIMEN

The material selected for the present investigation is oxygen-free copper of medium hardness supplied in 5 mm thickness and with a grain size of 20–30 μm. Pure copper is rarely selected for structural parts because of its mechanical properties. However, for the present investigation this material is attractive. Copper shows good ductility and takes relatively large plastic deformation at room temperature, it displays a great deal of elastic and plastic anisotropy on a microstructural level and has good neutron scattering properties, which is advantageous for the present experimental characterization of residual strains. Materials data have been extracted from tensile material tests according to DS/EN 10130 [2] and DS/EN 10002-1 [3]. The true stress–strain curve can be seen in Fig. 1. The sample geometry

was designed as a notched tensile test specimen with a very short gauge section, as shown in Fig. 2. Uniaxial deformation causes an inhomogeneous plastic deformation in the gauge section, leading to the generation of residual stresses across the specimen width upon unloading. Prior to deformation, samples were annealed at 450 °C for 30 min to reduce possible residual stresses generated when samples were manufactured. The samples were uniaxially loaded to an extension of 0.5 mm (measured between the dashed lines; see Fig. 2) and subsequently unloaded.

3 EXPLICIT FINITE ELEMENT ANALYSIS

When using an explicit FE method an acceleration of the computation is required to find a solution in reasonable CPU (central processing unit) time. One method is to increase the loading rate whereby the total number of time steps are decreased. However, when doing so care must be taken not to introduce any severe inertia or rate effects that are not part of the real process. One advantage of the explicit FE method is the fact that it does not involve iterations as it does when using an implicit FE method. This can save CPU time as well as hard disk storage. However, explicit codes are only conditionally stable, which means that only very small time steps, on the order of microseconds, are allowed. In the following a short introduction to the explicit FE method will be given; for further details see reference [4]. The implicit technique is well described in reference [5] and will not be touched upon here.

3.1 The explicit FE method

Explicit FE techniques are often built on a central difference scheme which explicitly solves the equation of motion with respect to the nodal displacements. The equation of motion at time t_n can be written as:

$$\mathbf{M}\ddot{\boldsymbol{d}}_n + \mathbf{C}\dot{\boldsymbol{d}}_n + \boldsymbol{F}_n^{\text{int}} = \boldsymbol{F}_n^{\text{ext}} \tag{1}$$

Here $\mathbf{M}$ is the mass matrix, $\mathbf{C}$ is the damping matrix and $\boldsymbol{F}_n^{\text{int}}$ and $\boldsymbol{F}_n^{\text{ext}}$ are the internal and external forces respectively.
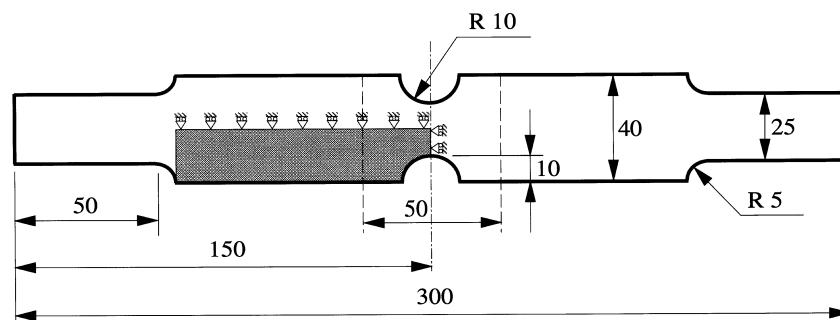

Fig. 2 Geometry and dimensions of the specimen, thickness 5 mm. In the finite element analysis only the shaded area of the specimen is modelled. Roller skates represent symmetry assumptions in the finite element model

Furthermore, $\ddot{d}_n$ and $\dot{d}_n$ are the acceleration and velocity vectors respectively. The central difference method can be derived from a Taylor series expansion around time step t_n to obtain the displacements:

$$d_{n+1} = d_n + \Delta t\, \dot{d}_n + \frac{\Delta t^2}{2}\ddot{d}_n + \frac{\Delta t^3}{6}\dddot{d}_n + \cdots \tag{2}$$

$$d_{n-1} = d_n - \Delta t\, \dot{d}_n + \frac{\Delta t^2}{2}\ddot{d}_n - \frac{\Delta t^3}{6}\dddot{d}_n + \cdots \tag{3}$$

By adding equations (2) and (3) an expression for the acceleration $\ddot{d}_n$ is obtained by a minor rearrangement of the new equation. Furthermore, subtraction of equation (3) from equation (2) gives an expression for the velocity $\dot{d}_n$; also, here a minor rearrangement is required. Terms containing Δt^3 and higher powers are omitted. The velocity and acceleration vectors are then given by the expressions:

$$\dot{d}_n = \frac{1}{2\Delta t}(d_{n+1} - d_{n-1}) \tag{4}$$

$$\ddot{d}_n = \frac{1}{(\Delta t)^2}(d_{n+1} - 2d_n + d_{n-1}) \tag{5}$$

Combining equations (1), (4) and (5) provides an equation for the external nodal forces at time step t_n:

$$F_n^{\text{ext}} = \mathbf{M}\left\{\frac{d_{n+1} - 2d_n + d_{n-1}}{\Delta t^2}\right\} + \mathbf{C}\left\{\frac{d_{n+1} - d_{n-1}}{2\Delta t}\right\} + F_n^{\text{int}} \tag{6}$$

The above approximation is only of second-order accuracy and has a finite stable time step (see Section 3.2), given by the Courant limit. After a minor rearrangement equation (6) provides an explicit expression for the displacement at time t_{n+1}:

$$d_{n+1} = \left\{\mathbf{M} + \frac{\Delta t}{2}\mathbf{C}\right\}^{-1}\left[(\Delta t)^2\left\{-F_n^{\text{int}} + F_n^{\text{ext}}\right\}\right.$$
$$\left. + 2\mathbf{M}d_n - \left\{\mathbf{M} - \frac{\Delta t}{2}\mathbf{C}\right\}d_{n-1}\right] \tag{7}$$

Now the displacements are expressed at time t_{n+1} in terms of the displacements at time steps t_n and t_{n-1}. Solving equation (7) is a simple task when the mass matrix $\mathbf{M}$ and the damping matrix $\mathbf{C}$ are diagonalized. The system of equations is uncoupled and it is not necessary to solve a set of equations simultaneously. However, certain precautions must be taken when the mass and damping matrices are established (see Section 3.3).

3.2 Critical time step

Only very small time steps, on the order of microseconds, are allowed in order to solve the equation of motion using the central difference method, as this method is only

conditionally stable. However, from a computationally economic point of view it is preferable to have as large time steps as possible. Implicit solvers do not have this disadvantage; here the time step is only limited by the required discretization in time. However, implicit solvers can cause convergence problems where explicit solvers do not. This justifies the use of an explicit FE technique in cases where implicit solvers can be expected to run into problems. The critical time step for an explicit FE scheme is given by

$$\Delta t \leqslant \frac{2}{\omega_{\max}} \tag{8}$$

where $\omega_{\max}$ is here the highest frequency of the determinant

$$\det(\mathbf{K} - \lambda\mathbf{M}) = 0 \tag{9}$$

The numerical results can be erroneous if the constraint of equation (8) is not fully satisfied. However, it is not convenient to calculate the highest frequency in this way as the stiffness matrix is not directly available and it would also make the computation time increase tremendously. To overcome this problem the critical time step is calculated as the Courant limit. The Courant limit is defined as the time in which an acoustic wave can propagate through an FE element in the mesh. The Courant limit is most easily explained from beam theory.

An estimate of the maximum frequency of the finite element mesh when the mass matrix of the system is lumped can be given as

$$\omega_{\max} = \frac{2c_i}{L_i} \tag{10}$$

where c_i is the acoustic wave speed through the ith element, which can be computed as

$$c_i = \sqrt{\left(\frac{E}{\rho_i}\right)} \tag{11}$$

and L_i is the length of the ith beam or truss element in the FE mesh. Thus, the Courant limit can be estimated by the expression

$$\Delta t_{\text{Courant}} = \frac{L_i}{c_i} \tag{12}$$

Keeping the time step below this limit will prevent the central difference method from becoming numerically unstable.

3.3 A lumped mass matrix

With a lumped mass matrix the equation of motion is uncoupled and it is not necessary to solve a set of equations simultaneously. A lumped mass matrix can be calculated as

$$\mathbf{M}_{\alpha i \beta j} = \delta_{\alpha\beta}\delta_{ij}\frac{1}{n_{\text{nodes}}}\sum_A \mathbf{M}_A \tag{13}$$

where αi refers to node α and the ith displacement and β refers to node β and the jth displacement. $\mathbf{M}_A$ is the mass of element A and n_{nodes} is the number of nodes in the element.

3.4 Increased loading rate

Using an increased loading rate decreases the total number of time steps in the computation. This can reduce the computation time significantly as it strongly depends on the number of time steps. Performing a typical deep drawing process takes 0.1–10 s and the simulation time will then typically be in the range 0.001–0.1 s. The operator has to verify that no severe rate or inertia effects have been introduced when using an increased loading rate. Another precaution to take when using an increased loading rate is to avoid introducing spurious high-frequency oscillation when using an inappropriate load function. Imposing load using step functions will introduce such unnecessary high-frequency oscillation. This effect can be significantly reduced by using a smooth load function where the load is imposed and removed gradually. In the present computations this has been utilized by means of a cosine function to specify the load–time relationship.

3.5 Mass scaling

Another method to reduce the computation time is to scale the mass matrix. This is done by minimizing the ratio between the lowest and the highest eigenfrequency of the finite element mesh. The method used in reference [6] is to scan the mass matrix $\mathbf{M}$ element by element to select a density for which the time step Δt_{nom} will be the same for all elements in the mesh. This is also called mesh homogenization and the density is then computed as

$$\Delta t_{nom} \leqslant \frac{L_i}{c_i} \tag{14}$$

which from equation (11) gives

$$\rho_i = \left(\frac{\Delta t_{nom}}{L_i}\right)^2 E \tag{15}$$

From the above equation a new element density is calculated. This element density is used for scaling the mass matrix in order to homogenize the finite element mesh with respect to the critical time step. When using mass scaling, errors may be introduced as the mass in the physical problem is rearranged, i.e. using higher and higher mass scaling will cause larger and larger transfer from the original physical problem to a non-physical problem. As is the case when increasing the loading rate, the operator will have to verify that no inertia effects are introduced when using mass scaling.

3.6 The FE model

For this analysis the explicit finite element code LS-Dyna3D, from Livermore Software Technology Corporation in the United States, has been used. The FE mesh of the test specimen can be seen in Fig. 3. As symmetry was assumed (see Fig. 2), only one-quarter of the specimen was modelled. The specimen is modelled in three dimensions and is composed of 4720 eight-node hexahedron solid elements with 24 degrees of freedom. There are five elements through the thickness. After plastic deformation artificial damping has been imposed on the model. This is used to damp out the dynamic response of elastic strains and stresses in the FE model. Applying it after the plastic distortion has ended prevents the results from being polluted by any plastic distortion caused by the artificial damping force. The von Mises isotropic yield criteria and a piecewise linear approximation of the true stress–strain curve with isotropic hardening have been used in the FE model. The mass was scaled by a factor of 3.7 and the loading rate was increased by a factor of 300.

All plastic distortion has been restrained to the notched area and during loading and unloading the specimen has
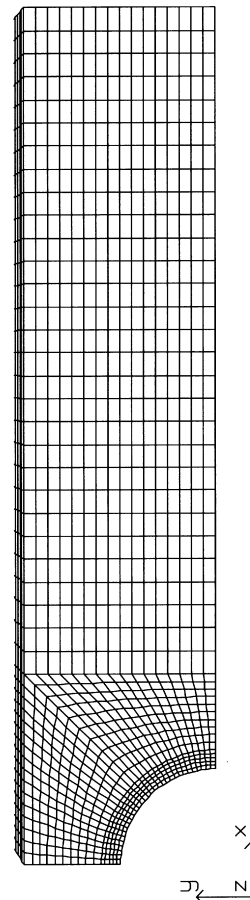

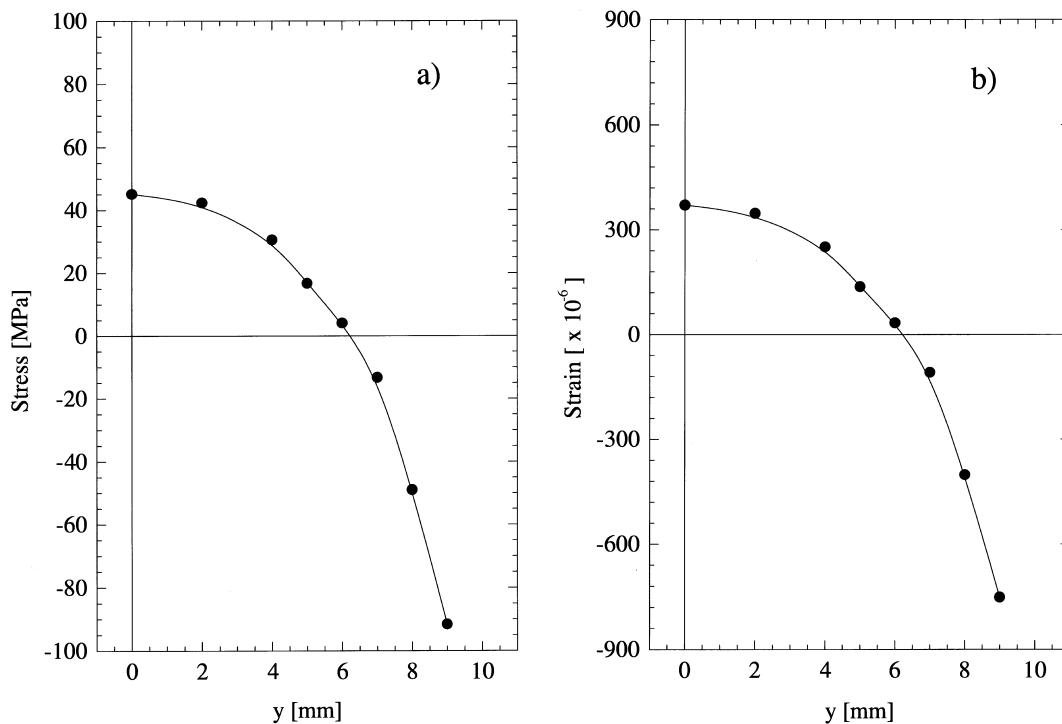**Fig. 3** FE mesh of the specimen, with five elements through the thickness

Fig. 4 (a) Residual *x*-stress and (b) residual elastic *x*-strain profiles along the symmetry plane $x = 0$

developed a non-homogeneous distribution of plastic strain-ing in the notched area. This non-homogeneous plastic straining causes the development of residual stresses in the same area. The computed residual stress and elastic strain profiles along the symmetry plane $x = 0$ are shown in Fig. 4.

4 NEUTRON DIFFRACTION

As an experimental means of evaluating the numerical predictions described above, neutron diffraction is utilized. Neutron diffraction for characterization of residual stresses and strains has been evolving during the past 15 years (see references [7], [8] and [9]), and is today an established non-destructive technique finding widespread use in material science as well as in engineering.

4.1 The neutron diffraction technique

The basis of the neutron diffraction technique is simple Bragg scattering, where selected lattice plane spacings, d^{hkl}, are measured. Comparing to some reference lattice plane spacing, d_0^{hkl}, a measure of the elastic strain is established as follows:

$$\varepsilon = \frac{d^{hkl} - d_0^{hkl}}{d_0^{hkl}}$$

As the penetration power of neutrons is on the order of centimetres in most common engineering materials, strains can

be evaluated non-destructively in bulk material. Furthermore, the gauge volume can be specified by an accurate definition of incident and diffracted beam lines, and the strain component of interest can be selected by proper orientation of the sample relative to the scattering vector. Due to the selective nature of the diffraction technique only the subset of grains with an orientation and lattice plane spacing fulfilling the Bragg condition is monitored.

4.2 Characterization of the lattice strain distribution

The neutron diffraction experiments were conducted on the TAS-8 instrument of the research reactor at Risø National Laboratory. Here the white neutron beam from the reactor is monochromatized using a graphite monochromator. The gauge volume is defined using slit systems in the incident and diffracted beam lines, and the sample positioning is done using an automated sample robot. The present investigation deals with the characterization of the distribution of lattice strains across the sample width at the notch and in a direction parallel to the deformation axis. The set-up is illustrated in Fig. 5 showing the gauge volume to cover the entire specimen thickness and covering 1 mm along the specimen width. As described in Section 4.1, specific (*hkl*) lattice planes are selected as the internal strain gauges, and for the present investigation the (111) and (200) reflections are selected. For each reflection the gauge volume was scanned half-way across the specimen width from the centre ($y = 0$) to the surface edge ($y = 10$), and the symmetry of the strain distribution was verified by two measurements at
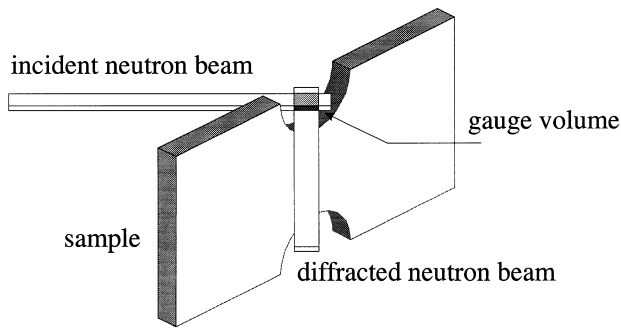
Fig. 5 Set-up for the neutron diffraction measurements of lattice strain distributions. The gauge volume is seen as the intersection of the incident and diffracted beams, and the mapping of strains is done by scanning the sample passing this gauge volume

negative *y* coordinates. As a reference for strain calculation (see above) the lattice parameter distribution of an undeformed sample was characterized. The results in terms of the elastic residual lattice strain distributions are presented in Fig. 6. It can be seen that the data from the two reflections differ noticeably with the results of the (200) reflection showing the greatest amplitude; both sets do, however, follow
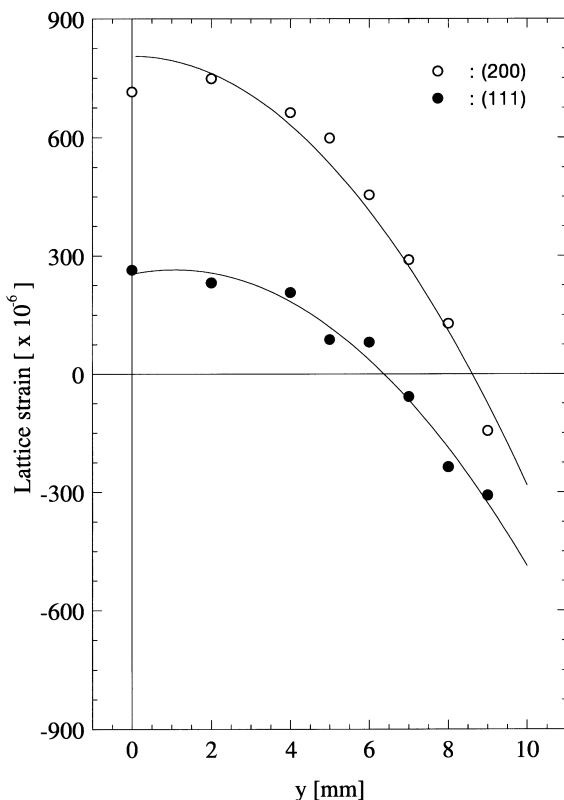
Fig. 6 Elastic residual lattice strain distribution across the sample width; solid lines are meant as guides to the eye

the expectations of the centre of the sample, being in tension, while the edge is in compression. From the present data it is evident that the interior deformation of the crystalline material is quite complicated and that continuum mechanics predictions are merely averages of the actual anisotropic micromechanical deformation of the polycrystalline aggregate. In order to deduce an engineering measure of the residual strain distribution from the present data, an accurate analysis is necessary, as described in Section 5 below.

5   ANALYSIS

The results presented in Fig. 6 clearly indicate that on a microstructural level the lattice strains in a polycrystalline aggregate of copper are quite anisotropic. Copper single crystals show a very large degree of elastic anisotropy with the ⟨111⟩ crystal direction having a Young's modulus of 191 GPa, whereas for the ⟨200⟩ direction it is 67 GPa [10]. These are the extremes [10] and the macroscopic modulus is found somewhere in between these values. Furthermore, plastic anisotropy on a grain-size scale causes the development of intergranular stresses and strains, as some grains, with certain orientations, deform plastically before others. The overall result of the deformation process is a balance between the elastic and plastic anisotropy where locally self-equilibrating intergranular residual stresses evolve due to the microstructural anisotropy, and different (*hkl*) reflections show different levels of residual lattice strain distributions as a result of the macroscopic inhomogeneity of the deformation process. The experimental data of Fig. 6 reflect the combined result of these effects and, for comparison with the continuum mechanics based FE predictions, it is necessary to separate the contributions of these intergranular effects.

5.1   Numerical and experimental predictions of intergranular strain effects

The local intergranular stresses and strains in the polycrystalline aggregate have been determined both numerically and experimentally. For the numerical predictions a self-consistent scheme [11] based on reference [12], where the polycrystalline aggregate is assumed to consist of an agglomerate of single crystals, was implemented. In this self-consistent modelling scheme each single crystal is considered as a spherical inclusion embedded in an effective medium with the elastic properties determined as the average of the complete set of crystallites in the agglomerate. The overall boundary conditions of the agglomerate are those of a uniaxial stress state, with all other tractions than the one along the deformation axis being equal to zero. Through an iteration procedure it is confirmed that when having considered all crystallites in the agglomerate the macroscopic deformation is consistent with these boundary conditions. Each single crystal deforms by crystallographic slip and accommodates the deformation by

Table 1 Elastic stiffnesses in characteristic directions of a copper single crystal, here compared to the Kröner averages for an untextured polycrystalline aggregate

	E_{111} (GPa)	E_{110} (GPa)	E_{200} (GPa)
Single crystals	191	130	67
Kröner estimates	150	137	99

combined slip on the usual $\{111\}\langle 110\rangle$ family of slip systems in crystals of the f.c.c. structure. Uniaxial deformation to 1, 1.8 and 2.4 per cent total strain were simulated, from which the elastic lattice strains in the subset of grains having their crystallographic $\langle 111\rangle$, $\langle 200\rangle$ or $\langle 220\rangle$ directions aligned along the deformation axis were selectively deduced. From the elastic part of the deformation the effective Kröner stiffness of these subsets [**13**] was deduced; the results are given in Table 1 together with the theoretical single-crystal values. The Kröner modulus should be used for the subsequent conversion of lattice strain distributions to stresses. The plastic part of the deformation gives rise to local self-equilibrating intergranular residual stresses and strains upon unloading. These predictions for the three reflections mentioned in Table 1 are shown in Fig. 7 in terms of an anisotropy factor (Γ) defined in the figure, which goes from 0 for the (100) reflection to 0.33 for the (111) reflection [**10**]. The subset of grains having their $\langle 200\rangle$ direction along the deformation axis returns into a state of residual tension upon unloading. So do the grains having their $\langle 111\rangle$ direction along the deformation axis, though to a smaller degree, whereas those with their $\langle 220\rangle$ direction along the deformation axis return into compression. Furthermore, it is noted that the numerical size of these local intergranular strains are of the order of $1-4\times 10^{-4}$. For a further description of

this numerical approach to the prediction of intergranular strains and stresses see reference [**14**]. In order to evaluate such numerical predictions neutron diffraction experiments are conducted. Using a stress rig developed for the TAS-8 spectrometer at Risø [**15**], the evolution of elastic lattice strains are followed during *in situ* uniaxial straining of small copper samples to 1 per cent total strain. The experimental results for the (111), (220) and (200) reflections are shown in Fig. 8 where the lines are merely meant as guides to the eye. The anisotropic evolution of lattice strains is clearly seen with the (200) reflection experiencing the largest lattice strains, whereas the (220) reflection shows a lattice strain evolution that is essentially linear, though with a tendency towards a slope of infinity which is indicating a saturation in the evolution of elastic strains. Upon unloading the development is observed of intergranular residual lattice strains with the (200) and (111) reflections returning into states of tension, while the (220) reflection returns into a state of compression, as illustrated by the numerical predictions shown in Fig. 7. In terms of the sign and order of magnitude of the residual intergranular lattice strains, these experimental observations substantiate the numerical predictions by the modelling approach, as described above and in Fig. 7. For a more detailed evaluation of the modelling schemes by direct experimental observations and for further information on the development of intergranular strains and stresses in f.c.c. polycrystals and the effect of elastic and plastic anisotropy see reference [**16**].

5.2 Modification of experimental strain profiles

As mentioned in Section 5, such intergranular strains ought to be subtracted numerically from the results of Fig. 6 when comparing with an engineering estimate given by the FE calculations. In fact, the level of intergranular strains to be
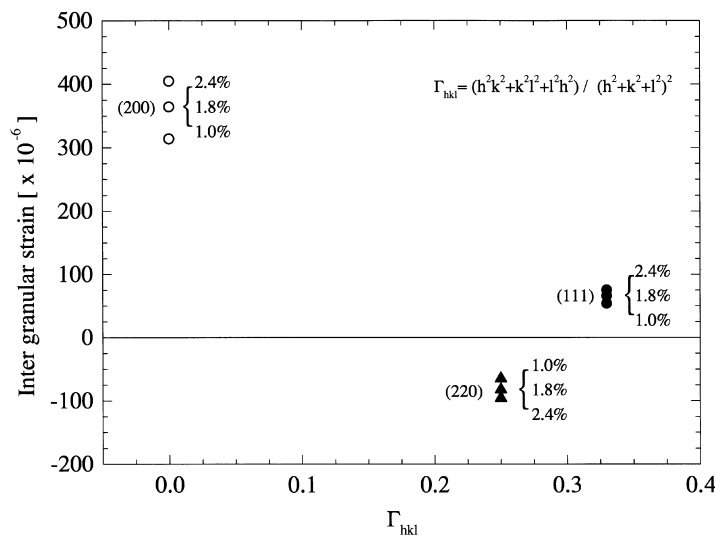
Fig. 7 Numerical predictions of the intergranular residual strains after 1, 1.8 and 2.4 per cent total deformation, here given as a function of the Γ parameter defined in the graph
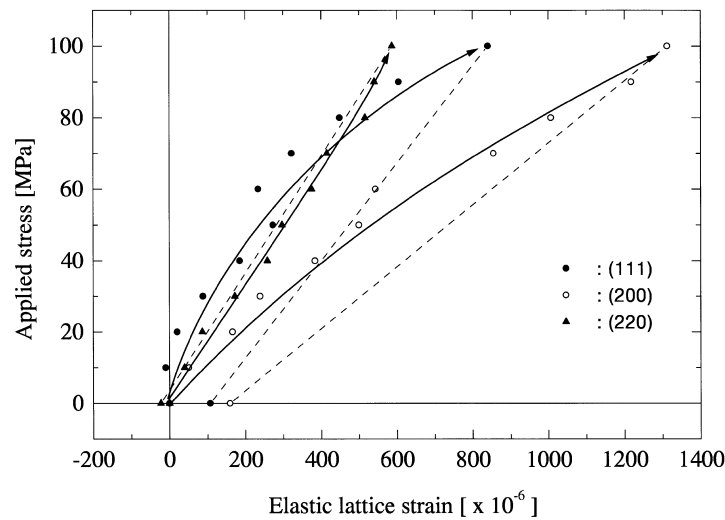
Fig. 8 *In situ* neutron diffraction characterization of lattice strains during uniaxial straining of small tensile specimens

subtracted depends on the degree of plastic deformation and hence varies across the specimen width. The present FE predictions show that the entire sample cross-section experiences plastic deformation, with the maximum being 2.4 per cent at the sample edge ($y = 10$) and the minimum being 1.8 per cent at the sample centre ($y = 0$). For the present analysis the intergranular strains are assumed to vary linearly from the sample edge to the sample centre using the numerically predicted levels for 2.4 and 1.8 per cent plastic strain. The data from Fig. 6 are subsequently modified by these intergranular strains and the resulting profiles are shown in Fig. 9.

5.3   Comparison of FE and neutron diffraction results

In the present case experimental results are only available in terms of the x component of residual elastic lattice strains, and hence the comparisons to be made are based on this component alone. From the detailed numerical results the average values can be deduced for regions corresponding to the gauge volumes used in the neutron diffraction experiments. The numerical results are presented in Fig. 9 together with the residual elastic strain profiles measured using the (111) and the (200) reflections. It is observed that both sets of experimental results follow the trend of the numerical predictions. Note that in particular the (200) reflection follows closely the numerical predictions, though some differences are observed especially near the outer edge at $y = 10$ mm. The stiff (111) reflection is typically monitoring numerically lower strains as calculated. It is in particular worth while noticing, when comparing the numerical predictions with the experimental results prior to being modified by the residual intergranular strains (see Fig. 6), that the differences here are far greater. Especially the (200) reflection, which is strongly affected by residual
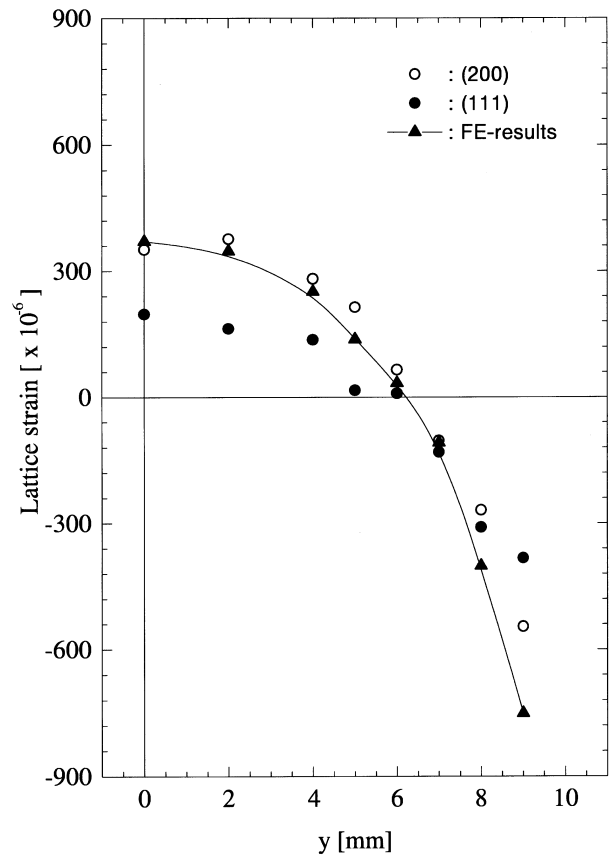
Fig. 9 Lattice strain distributions of the (111) and the (200) reflections now modified by the intergranular strains as calculated by a self-consistent modelling scheme and compared to the FE results

intergranular strains, shows results that differ greatly from the numerical predictions.

6 CONCLUSIONS

In the present investigation a simple sample geometry and a simple deformation mode which was simulated by explicit FE calculations were deliberately selected. The numerical results have been verified by non-destructive neutron diffraction characterization of the residual lattice strains. By means of this diffraction technique, which probes the elastic lattice strains in selected subsets of grains, it has been verified that on a microstructural level there is a noticeable degree of anisotropy in stresses and strains. By a self-consistent modelling scheme the levels of intergranular strains generated during plastic deformation have been determined, and the numerical results have been substantiated by neutron diffraction. Through the analysis of the experimental data it has been shown how to separate these intergranular residual strains from those arising from the macroscopic inhomogeneity of the deformation, and residual strain profiles, used to validate the accuracy of the FE predictions, have been determined experimentally.

The experimental results for the notched specimen show that the grains oriented with their crystallographic ⟨200⟩ direction along the deformation axis experience much higher residual strains than those with their ⟨111⟩ direction along this axis. Hence, the results display the balance between elastic and plastic anisotropy present on a microstructural level in a polycrystal, information that is not revealed through continuum mechanics-based FE simulations.

The observed differences between numerical predictions and experimental observations in Section 5 are not meant to judge the correctness of one approach or the other. Rather, the essential conclusion to be drawn is that a firm understanding of the anisotropy effects present on a microstructural level is necessary for a fair comparison with a continuum mechanics-based numerical technique. Through this understanding the experimental observations can be modified in order to render results that resemble the numerical predictions. However, this does not remove the truth in the observations presented in Fig. 6 that the (200) oriented grains in the aggregate are strained to far higher levels than the macroscopic average predicted by the continuum mechanics-based technique. In the centre of the specimen the (200) oriented grains are in fact observing strains in excess of two times those of the numerical predictions. Such high local strains levels ought to be of importance for more fatigue and damage oriented aspects of materials; such aspects are, however, beyond the scope of the present investigation.

The present investigation, and especially the presented analysis of diffraction results, will in future work be utilized for more complicated parts and deformation processes, with the ultimate goal being a validation of the capabilities of the explicit FE technique for predicting residual stresses in sheet metal forming operations.

ACKNOWLEDGEMENT

REFERENCES

1 **Allen, A. J., Hutchings, M. T., Windsor, C. G.** and **Andreani, C.** Neutron diffraction methods for the study of residual stress fields. *Adv. Physics*, 1985, **34**(4), 445–473.

2 **DS/EN 10130**. Cold rolled low carbon steel flat products for cold forming—technical delivery conditions. European Committee for Standardisation, March 1991.

3 **DS/EN 10002**. Metallic materials—tensile testing. Part 1: method and test (at ambient temperature). European Committee for Standardisation, March 1990.

4 **Benson, D. J.** Computational methods in Langrangian and Eulerian hydrocodes. *Comput. Meth. Appl. Mechanics and Engng*, 1992, **99**, 235–394.

5 **Crisfield, M. A.** *Non-linear Finite Element Analysis of Solids and Structures*, Vol 1, *Essentials*, 1991, p. 15 (John Wiley, Chichester).

6 **Nielsen, K. B., Brännberg, N.** and **Nilson L.** Sheet metal forming simulation using explicit finite element methods. In Proceedings of EURODYN '93, Norway, 21–23 June 1993, pp. 625–633.

7 **Allen, A. J., Andreani, C., Hutchings, M. T.** and **Windsor, C. G.** Measurements of internal stresses within bulk materials using neutron diffraction. In NDT-International, October 1981, pp. 249–254.

8 **Krawitz, A. D., Brune, J. E.** and **Schmank, M. J.** Measurements of stress in the interior of solids with neutrons. In Proceedings of the 28th Sagamore Army Materials Research Conference on *Residual Stress and Stress Relaxation* (Eds E. Kula and V. Weiss), Lake Placid, New York, 1981, pp. l39–155 (Plenum Press, New York).

9 **Pintschovious, L., Jung, V., Macherauch, E., Schäfer, R.** and **Vöhringer, O.** Determination of residual stress distributions in the interior of technical parts by means of neutron diffraction. In Proceedings of the 28th Sagamore Army Materials Research Conference on *Residual Stress and Stress Relaxation* (Eds E. Kula and V. Weiss), Lake Placid, New York, 1981, pp. 467–482 (Plenum Press, New York).

10 **Noyan, I. C.** and **Cohen, J. B.** *Residual Stress, Measurement by Diffraction and Interpretation*, MRE Materials Research and Engineering, 1987 (Springer-Verlag, New York).

11 **Clausen, B.** and **Lorentzen, T.** A self-consistent model for polycrystal deformation, description and implementation. Risø-R-970(EN), Risø National Laboratory, Roskilde, Denmark, 1997.

12 **Hutchingson, J. W.** Elastic–plastic behaviour of polycrystalline metals and composites. *Proc. R. Soc., Lond.*, 1970, **A319**, 247–272.

13 Kröner, E. *Physik*, 1958, **151**, 504–518.

14 Clausen, B. and **Lorentzen, T.** Experimental evaluation of a polycrystal deformation modelling scheme using neutron diffraction measurements. *Metall. Trans. A*, 1997, **28A**, 2537–2541.

15 Lorentzen, T. and **Sørensen, N. J.** A new device for in-situ loading of samples during neutron diffraction strain measurements. In *Metal Matrix Composites—Processing, Microstructure and Properties*, 12th Risø International Symposium on *Materials Science* (Eds N. Hansen, D. Juul Jensen, T. Leffers, H. Lilholt, T. Lorentzen, O. B. Pedersen and B. Ralph), Risø National Laboratory, Roskilde, Denmark, 1991, pp. 489–496.

16 Clausen, B., Lorentzen, T. and **Leffers, T.** Self-consistent modelling of the plastic deformation of fcc polyscrystals and its implications for the diffraction measurements of residual/internal stresses. *Acta Mater.*, 1998, **46**(9), 3087–3098.